Plasma Transferred Arc Repair Welding of the Nickel-Base Superalloy IN-738LC

C.Y. Su, C.P. Chou, B.C. Wu, and W.C. Lih

Plasma transferred arc welding (PTA) has been considered a promising process to restore worn areas of land-based gas turbine blades and vanes.

The objective of this investigation was to study the effect of PTA welding on the repairing of IN-738LC superalloy components. Tensile tests were conducted on specimens welded with various combinations of parameters. Room temperature, 760 °C, and 980 °C were selected as tensile test temperatures. High-temperature phase transformed, during solidification, were identified by differential thermal analysis (DTA). The weld-pool shapes and microstructures of welded specimens prepared by various welding parameters were evaluated by optical metallography (OM), a scanning electron microscope (SEM) equipped with energy dispersive x-ray spectrometer (EDS), and microhardness testing.

Results of this study showed that PTA welded specimens exhibited 96% nominal tensile strength of IN-738LC base materials. Specimen failure was observed predominantly in the base materials instead of in the heat-affected zone (HAZ) for gas tungsten arc weld (GTAW) repair weldments. IN-738LC is considered susceptible to weld cracking during fusion welding; however, using a low-input heat repair welding process (PTA), cracking susceptibility could be minimized by the optimized welding parameters.

Keywords IN-738LC, Ni-base alloy, plasma, welding

1. Introduction

IN-738LC, which is a γ' precipitation-hardening nickel-base superalloy, has been extensively used as land-based gas turbine blade/vane materials.

In general, superalloys were considered difficult to weld, especially those exhibiting precipitation-hardening reactions involving titanium and/or aluminum (Ref 1). Microfissures have been observed to occur in the welded metal and the heat-affected zone (HAZ) during welding and during the subsequent postweld heat treatment (Ref 1-4). Heat-affected zone cracking was attributed to liquation cracking and a subsolidus ductility dip (Ref 5-7). In the first type, cracking is proposed to occur during the final stages of solidification of the thin liquid films formed on HAZ grain boundaries. Two different mechanisms have been proposed for the origin of the liquid film on the grain boundaries: (1) grain-boundary melting caused by local compositional variations arising from segregation and (2) liquid film formation on grain boundaries caused by the constitutional liquation of primary carbides and carbonitrides, borides, sulfides, and so forth. It has been suggested that the second type of HAZ cracking occurs in the solid state exhibiting a drop in ductility below the solidus temperature.

It is shown in Fig. 1 (Ref 8), indicating that the tendency of strain-age cracking depends on the total titanium and aluminum content for several nickel-base superalloys. According to Prager's study (Ref 8), the weldability of the IN-738LC is poor and not suitable for fusion welding. Jahnke (Ref 9) employed high preheat temperature (1120 °C) of electron beam (EB) welding to reduce the microfissuring of postweld IN-738LC. Lowering the welding energy input may decrease the tendency of cracking. The lower heat input reduces the volume of weld metal that undergoes shrinkage during cooling, therefore reduces the thermal strain, and consequently decreases the cracking sensitivity. Electron beam welding exhibited very low heat inputs; however, this process must proceed in high vacuum and is generally not economical.

The purpose of this study was to apply plasma transferred arc welding (PTA), which was considered an energy con-

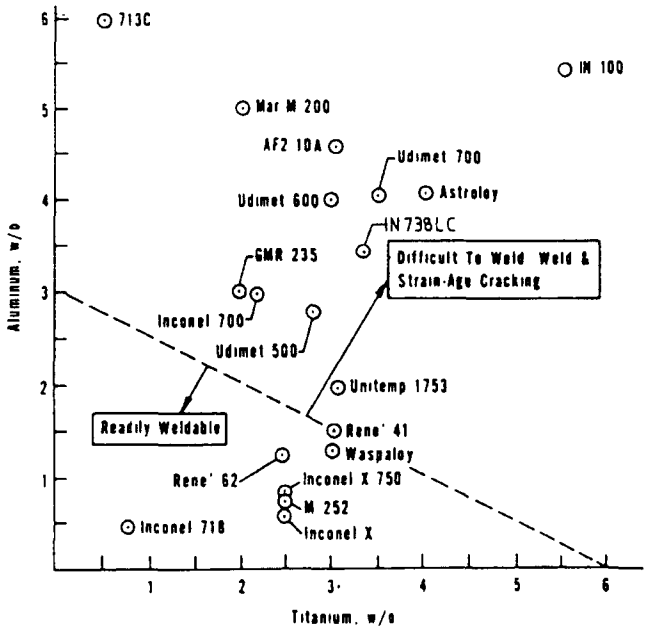

Fig. 1 Prager's plot of weldability versus aluminum and titanium content, with several current cast nickel-base superalloys added, based on strain-age cracking susceptibility (Ref 8)

C.Y. Su and **C.P. Chou,** Department of Mechanical Engineering, National Chiao Tung University, Hsinchu, Taiwan, R.O.C.; and **B.C. Wu** and **W.C. Lih,** Industrial Technology Research Institute, Materials Research Laboratories, Hsinchu, Taiwan, R.O.C.

stricted and concentrated process, on IN-738LC plates to result in lower heat inputs. The filler metal of PTA is in powder form and was added directly into PTA torch. As a result, lower dilution and high deposition rate were also expected as the advantages of PTA process for IN-738LC components repairs.

2. Materials and Experimental Procedures

The base metal used in this study was IN-738LC nickel-base superalloy. The compositions of the alloy were determined using inductively coupled plasma-atomic emission spectroscopy

Table 1 Compositions of IN-738LC by ICP-AES detection

	Composition, wt%											
	Cr	Co	Al	Ti	Al + Ti	Mo	W	Ta	Nb	C	B	Ni
Base metal	13.87	7.14	3.08	3.34	6.42	1.50	2.79	2.27	0.77	(a)	(a)	Bal
PRAXAIR NI-284-1	16.44	8.52	3.56	3.76	7.32	1.76	3.21	2.63	0.98	(a)	(a)	Bal

(a) Did not detect

Table 2 Welding parameters

Specimen No.(a)	Current, A	Voltage, V	Travel speed, mm/min	Powder feed rate, g/min	RWHT
GE1_85	85	23.4	240	8	yes
GE1_100	100	24.3	240	8	yes
GE1_115	115	25.3	240	8	yes
GE2_55	55	21.6	169	5.6	yes
GE2_70	70	22.5	169	5.6	yes
GE2_90	90	23.7	169	5.6	yes
GE3_85	85	23.4	240	8	no
GE3_100	100	24.3	240	8	no
GE3_115	115	25.3	240	8	no
GE4_55	55	21.6	169	5.6	no
GE4_70	70	22.5	169	5.6	no
GE4_90	90	23.7	169	5.6	no
DE1_50	50	21.3	240	8	yes
DE1_70	70	22.5	240	8	yes
DE1_90	90	23.7	240	8	yes
DE3_50	50	21.3	240	8	no
DE3_70	70	22.5	240	8	no
DE3_90	90	23.7	240	8	no

Note: arc length: 10 mm, electrode diameter (tungsten): 0.125 in. (3 mm) nominal, plasma gas fluid rate: 3 ft^3/h (0.023 L/s), protective gas: argon, preweld heat treatment (RWHT): 1120 °C/2 h, AC, postweld heat treatment (PWHT): 1120 °C/2 h, AC and 845 °C/24 h, AC. (a) GE is the joint weld; DE is the deposition weld.

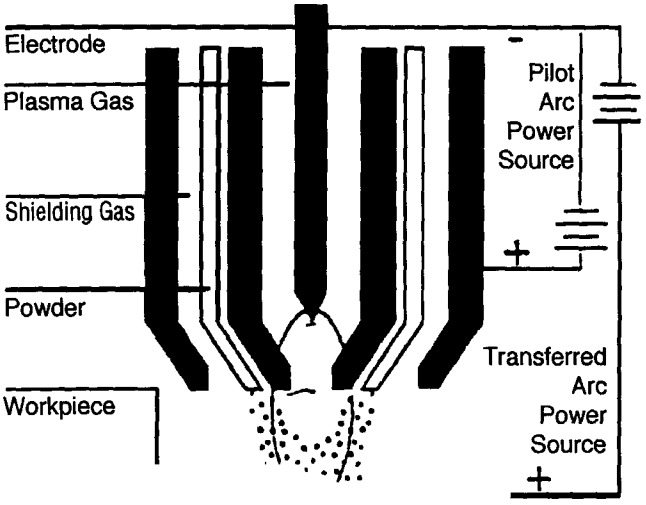

Fig. 2 The torch mechanism of PTA (Ref 10)

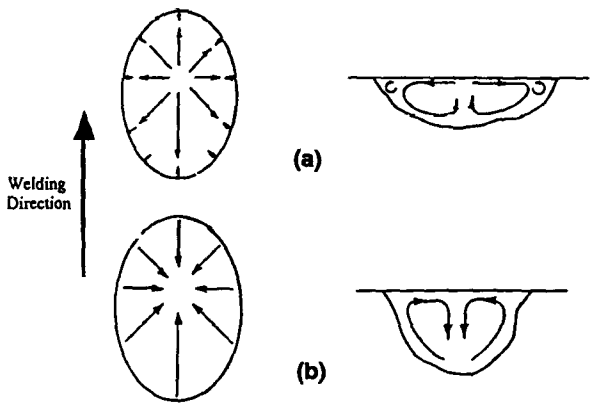

Fig. 3 Proposed (Ref 12) surface and subsurface fluid flow in the weld pool. A, surface tension temperature coefficient negative; B, positive surface tension temperature coefficient

(ICP-AES) and is shown in Table 1. The IN-738LC plates were sliced from damaged Asea-Brown-Boveri (ABB) land-based gas turbine vanes root with 3 mm thickness. PRAXAIR NI-284-1 (Praxair Surface Technologies, Inc., Indianapolis, IN) was selected as feed powder.

The PTA system used was Starweld 3 by Stellite Company with Model 600 Torch.

In order to investigate the potential of repairing blades using a PTA system (Fig. 2), two groups of specimens were welded as follows: (1) direct deposited weld designed to simulate hot corrosion damage of blade surface, and hence restore the original blades and (2) null gap joint weld designed to simulate the penetrated cracking of mechanical stress. The parameters of this experiment are given in Table 2. The deposited rate of filler metal was fixed. Prior to welding, the samples were either in the as-cut condition for the root of the damaged blades and in the solution-treated condition as shown in Table 2. Postweld heat treatment was performed on all welded samples (Ref 11).

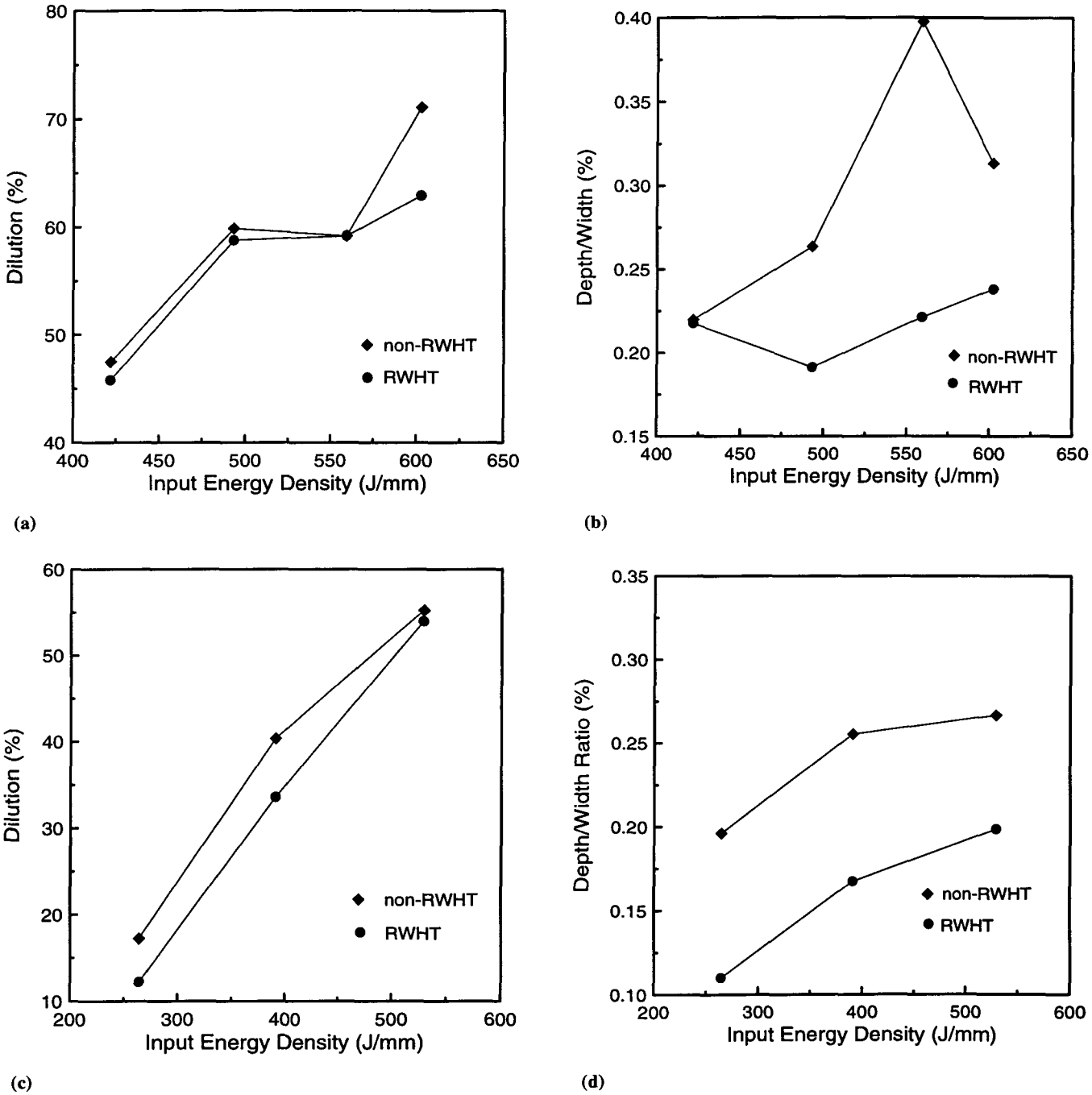

Fig. 4 (a) Weld dilution versus weld input energy density for the non-RWHT and RWHT specimens in the joint type. (b) Weld depth/width ratio versus weld input energy density for the non-RWHT and RWHT specimens in the joint type. (c) Weld dilution versus weld input energy density for the non-RWHT and RWHT specimens in the deposition type. (d) Weld depth/width ratio versus weld input energy density for the non-RWHT and RWHT specimens in the deposition type

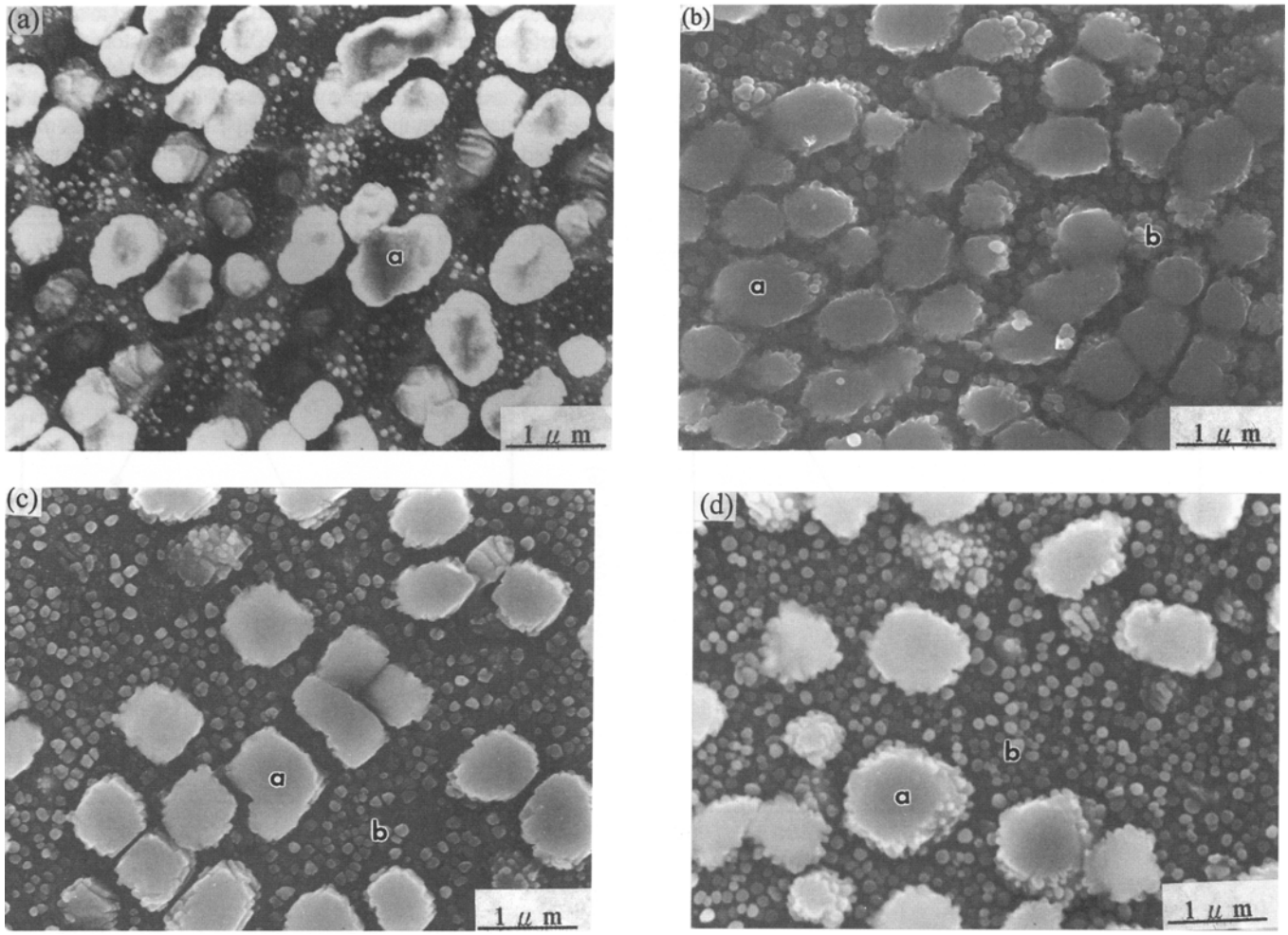

Fig. 5 The γ' distribution in base materials with different heat treatment (SEM). a, coarse γ'; b, cooling γ'. (a) non-RWHT and non-PWHT. (b) non-RWHT and PWHT. (c) RWHT and non-PWHT. (d) RWHT and PWHT

Differential thermal analysis (DTA) test was performed using a DuPont Thermal Analyzer 2000 (TA Instrument, Inc., Castle, DE) with empty alumina cup as a reference. Samples of as-received material, approximately 40 mg, were heated to 1500 °C at a rate of 0.33 °C/s during heating and cooling under flowing high-purity argon while solidification data were recorded.

Tensile test specimens were machined from welded sample according to ASTM E 8M. Tensile tests were performed at room temperature, 760 °C, and 980 °C with a strain rate of 0.04 mm/s.

The electrolytic etchant used for IN-738LC was 10 mL H_3PO_4, 45 mL H_2SO_4, and 45 mL HNO_3 at 6 Vdc for revealing the microstructure. Metallographic observation was performed in the fusion zone, the HAZ, and the base materials. An image analyzer was used to calculate the dilution rate and depth/width ratio of the fusion zone. Scanning electron microscopy was used to measure γ' size and distribution. A JEOL 840 scanning electron microscope (JEOL Ltd., Tokyo) equipped with an OXFORD energy-dispersive spectroscopy (EDS) system (Oxford Instruments Microanalysis Group, High Wycombe Bucks, England) with a LINK detector window (Oxford Instruments Microanalysis Group, High Wycombe Bucks, England) enabled a qualitative analysis of light elements such as carbon and nitrogen. Volume fraction of microstructural constituents were measured using an OPTIMUM Image Analyzer(BioScan,Incorporated,Edmonds,WA).

3. Results and Discussion

3.1 *Effect of Welding Parameters*

Shallow welds are observed for many alloys because in these materials the surface tension has a negative temperature coefficient. The surface tension gradient drives fluid flow from the center of the pool outward, as illustrated in Fig. 3(a). The outward fluid flow provides substantially greater heat transport to the outside of the pool. Figure 3(b) shows the surface tension temperature coefficient is positive.

Weld cross-sectional area, width, and depth of weld bead were measured by image analyzer. The effect of input energy density on the dilution and depth/width ratio for both the joint type and the deposition type are shown in Fig. 4. It is shown that both dilution and depth/width ratio increased as input energy density increased for both types. That is, weld depth increased

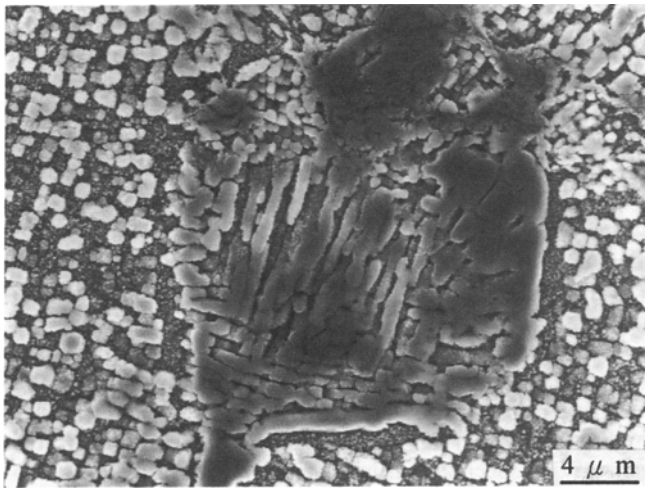

Fig. 6 The γ-γ′ eutectic phase of base material precipitated in grain boundary after high-temperature exposure for a long period (SEM)

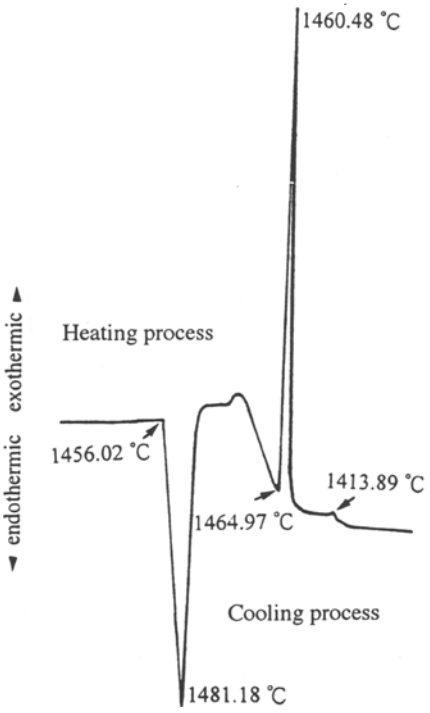

Fig. 8 DTA thermogram for filler metal IN-738LC

faster than weld width. It was proposed that the positive surface tension temperature coefficient dominates the flow model of filler materials in the weld (Ref 12). It was also proved that porosity might be minimized when this flow model takes place in the weld (Ref 13). This mechanism was also proved by microstructural investigation of PTA weld in this study, which showed that porosity was minimal.

For the joint specimen that was not heat treated before welding, the depth/width ratio decreased as the input energy density exceeded 559.2 J/mm. This is indicated in Fig. 4(b), and it can be proved that the surface tension temperature coefficient turns to negative. The results of Fig. 4(b) indicate that preweld heat treatment (RWHT) is important to keep the depth/width ratio within a controlled range that may benefit the weldability/repairability. On the other hand, for non-RWHT IN-738LC components, weldability may be susceptible to the degraded microstructure caused by long-term high-temperature operation, and this is discussed in section 3.2.

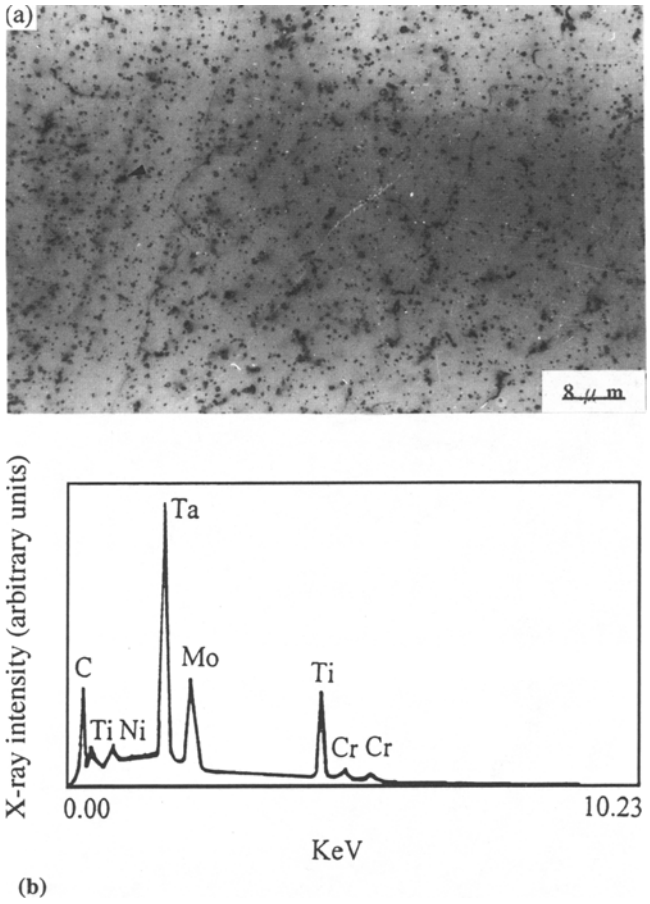

Fig. 7 Point carbide existed at dendritic intergranular region of as-welded metal. Welding current: 90 A, travel speed: 240 mm/min. (a) Light micrograph. 800 ×. (b) SEM-EDS analyses of the carbide in the dendrite intergranular

3.2 *Metallographic Investigation*

The size and distribution of γ′ phase in RWHT IN-738LC specimens are shown in Fig. 5. Coarse γ′ precipitate occurred after long-term high-temperature operation. It was observed in Fig. 5(c) that fine-cooled γ′ precipitated at the matrix of coarse γ′ for RWHT specimen. For postweld heat treatment (PWHT) specimens, coarse γ′, precipitated γ′, and cooled γ′ were all observed as presented in Fig. 5(b) and (d). The major purpose of RWHT is to release the accumulated stress and redissolve the segregation in IN-738LC cast after long-term operation and hence homogenize the matrix of IN-738LC to minimize the possibility of welding hot cracking. As shown in Fig. 6, γ-γ′ eutectic phase generally segregates at grain boundaries. Hot cracking and strain-aging cracking during repair welding are easily induced in this region due to the high hardness character of γ-γ′ eutectics.

Figure 7(a) shows the microstructure of RWHT welded metal for which welding current was 90 A, travel speed of 240

mm/min, and powder feed rate of 8 g/min. The black spotty precipitates around the dendrites observed in Fig. 7(a) were identified as carbides with tantalum, molybdenum, and titanium as main constituents.

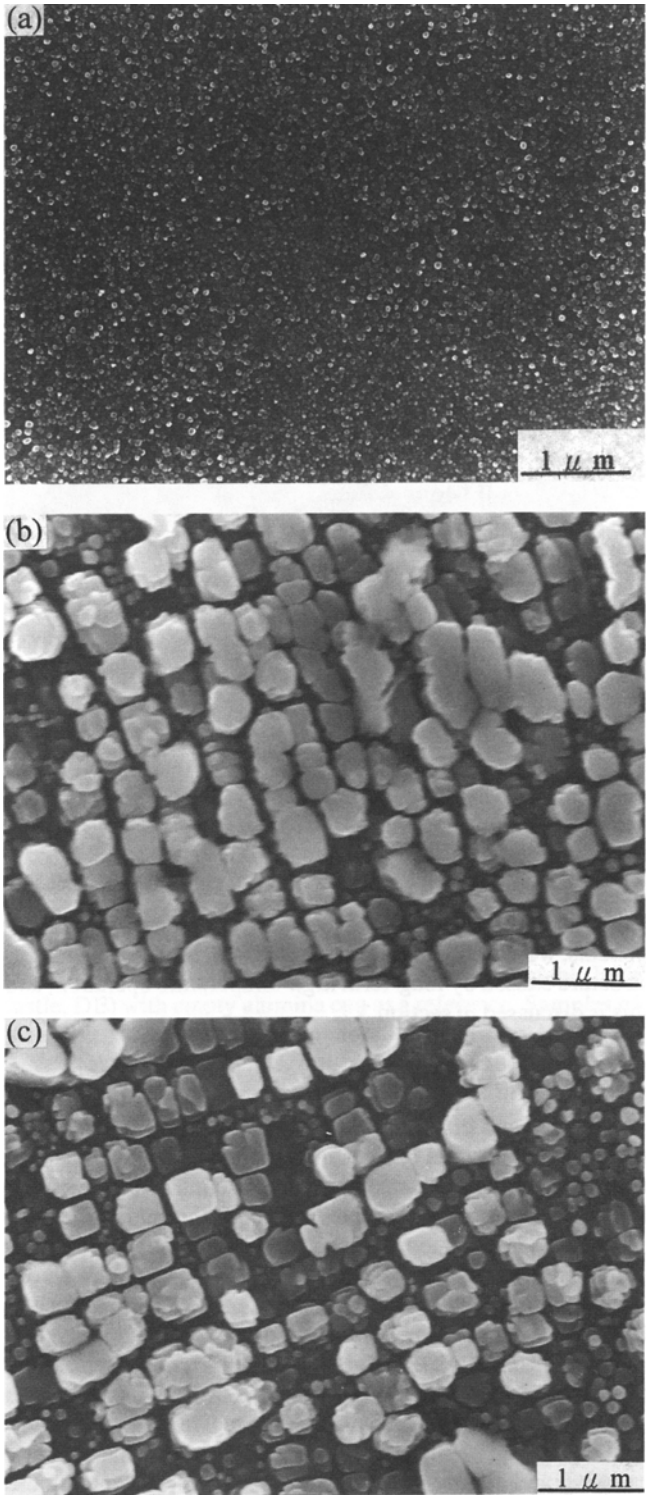

Fig. 9 The γ' distribution in the fusion zone with different heat treatment (SEM). Welding current: 90 A, travel speed: 240 mm/min. (a) non-RWHT and non-PWHT. (b) non-RWHT and PWHT. (c) RWHT and PWHT

Figure 8 shows the DTA thermograms of IN-738LC filler powder. The solidus temperature 1456 °C was identified by the initial deviation from the local baseline, and the liquidus temperature was determined as 1481 °C by the peaks on thermogram. There is at least one minor constituent solidification also identified at 1413 °C in DTA thermogram.

Figure 9 shows the microstructures of the PTA IN-738LC welds. For non-RWHT and non-PWHT welds, γ' precipitates were not observed; however, for both non-RWHT/PWHT and RWHT/PWHT welds γ' precipitates were observed in a homogeneous distribution.

The effects of RWHT and PWHT treatments on the hardness of both joint and deposition welds are shown in Fig. 10(a) and (b), respectively. The weld hardness is comparatively higher for joint RWHT specimens than the hardness for joint non-RWHT specimens as indicated in Fig. 10(a). This is tentatively to be inferred as the result of discontinuous carbides precipitated at finer dendrites of RWHT specimens, whereas the discontinuous carbides for non-RWHT specimens precipitated with coarser dendrites. Similar results of weld hardness were observed for deposition specimens, as shown in Fig. 10(b).

Liquation cracking is believed (Ref 13) to be associated with local or partial melting in the grain boundary adjacent to the fusion line in the HAZ. As shown in Fig. 11, partial melting was observed in the HAZ and believed to induce the microfissure from HAZ to the dendrite boundaries of fusion zone. Solute segregation at grain boundaries plays an important role in the type of localized melting as shown in Fig. 11. The distribution of γ' precipitates in the HAZ is shown in Fig. 12. For non-RWHT/non-PWHT specimen, γ' in HAZ were coarsened and hence coalesced. However, for RWHT/PWHT specimen, coarsened γ', cooled γ', and age precipitated γ' are observed incidentally as shown in Fig. 12(b). This indicates that part of the HAZ was remelted during welding and new γ' phase precipitated during cooling.

Weld cracking was not observed in this study due to the choice of low current/high travel speed of PTA torch parameters.

3.3 *Mechanical Property*

The results of tensile tests are shown in Fig. 13. At 760 and 980 °C, joint PTA specimens exhibited similar ultimate tensile strengths as base metal. However, for tensile tests at room temperature, the joint PTA specimen exhibited 80% of the ultimate tensile strength of the base metal.

Fracture failure was observed predominantly in the base materials and occasionally occur in the HAZ.

4. Conclusions

- Using plasma transferred arc welding, cast nickel-base superalloys, especially IN-738LC, can be welded without deleterious HAZ or weld metal cracking.
- Weld cross-sectional analysis showed that preweld heat treatment could improve the weldability of joint IN-738LC components by long-term high-temperature operation.
- Metallographic inspection showed a very fine dendritic solidification structure. Using proper postweld heat treatment, the distribution of γ' precipitates can become homogeneous.

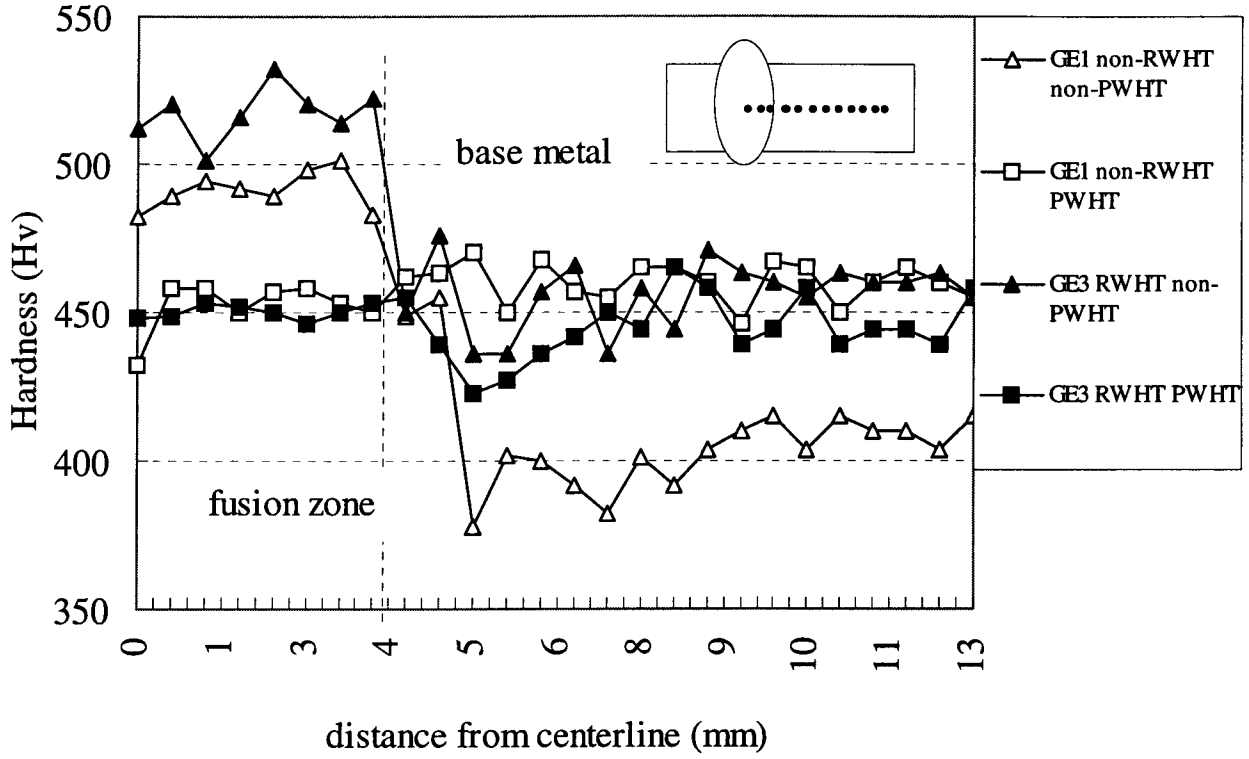

(a)

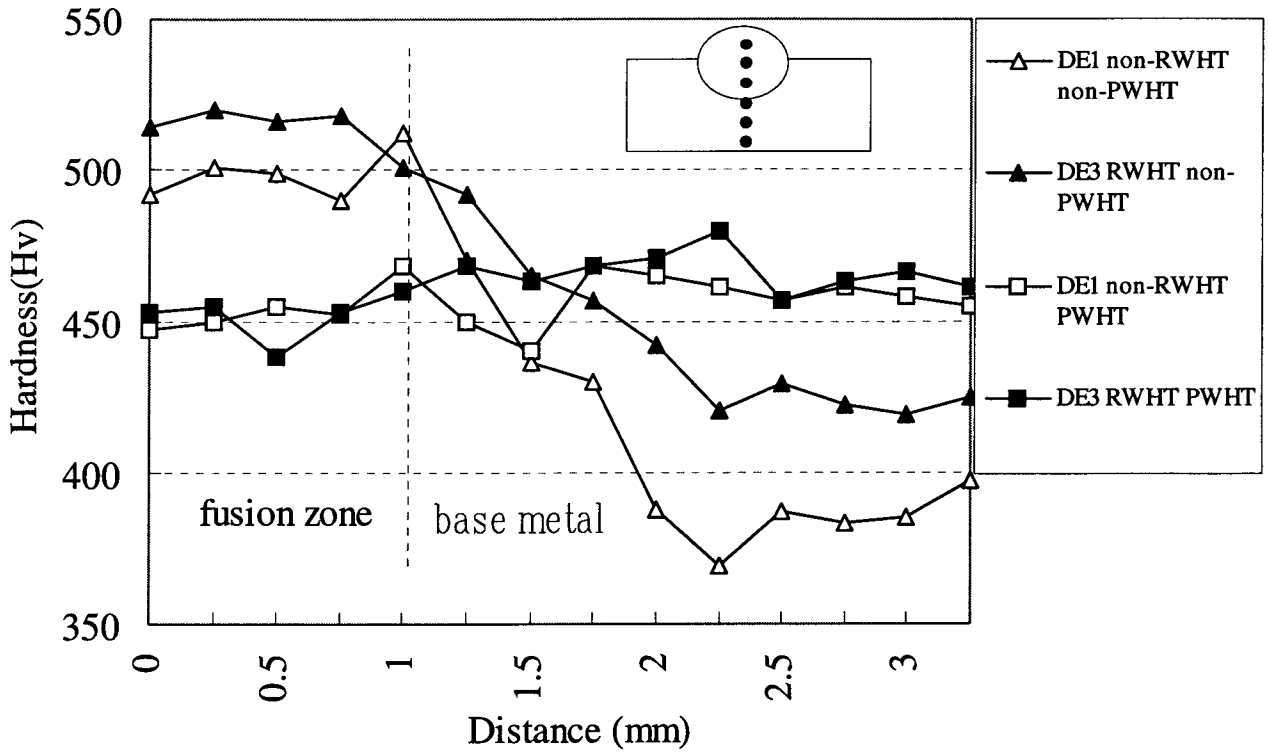

(b)

Fig. 10 (a) Microhardness distribution curve across PTA fusion zone in the joint type. Welding parameters: current, 115 A; voltage, 25.3 V; speed, 240 mm/min; powder rate, 8 gw/min. Hardness test load is 200 g. (b) Microhardness distribution curve across PTA fusion zone in the deposition type. Welding parameters: current, 50 A; voltage, 21.3 V; speed, 240 mm/min; powder rate, 8 gw/min. Hardness test load is 200 g.

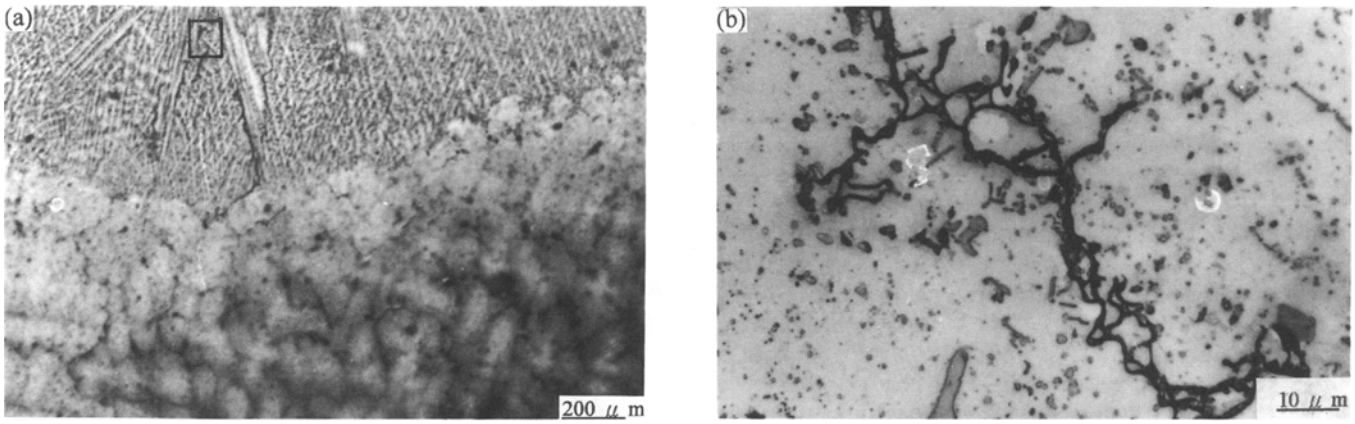

Fig. 11 Liquation cracking of fusion zone induced from the partial melting zone, welding current: 90 A, welding speed: 240 mm/min, non-RWHT (OM)

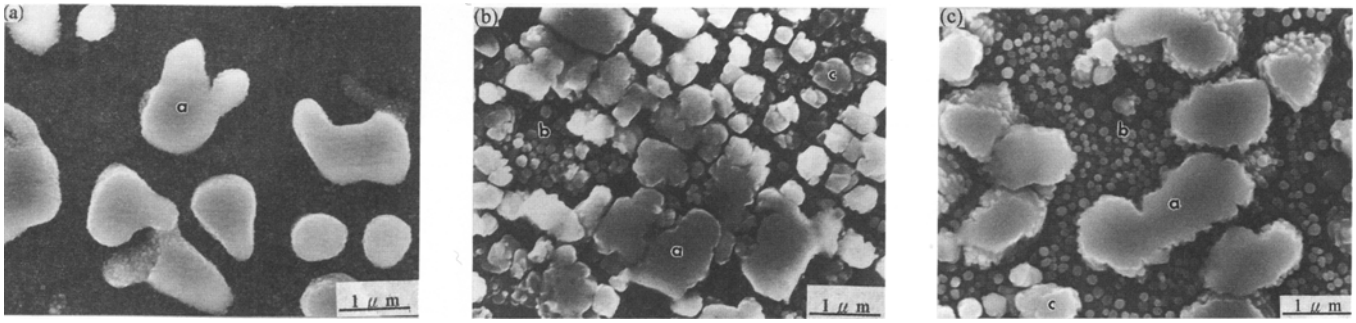

Fig. 12 The γ' distribution of HAZ was differently heat treated (SEM). Welding current: 90 A, travel speed: 240 mm/min (Ref 11). (a) non-RWHT and non-PWHT. (b) non-RWHT and PWHT. (c) RWHT and PWHT

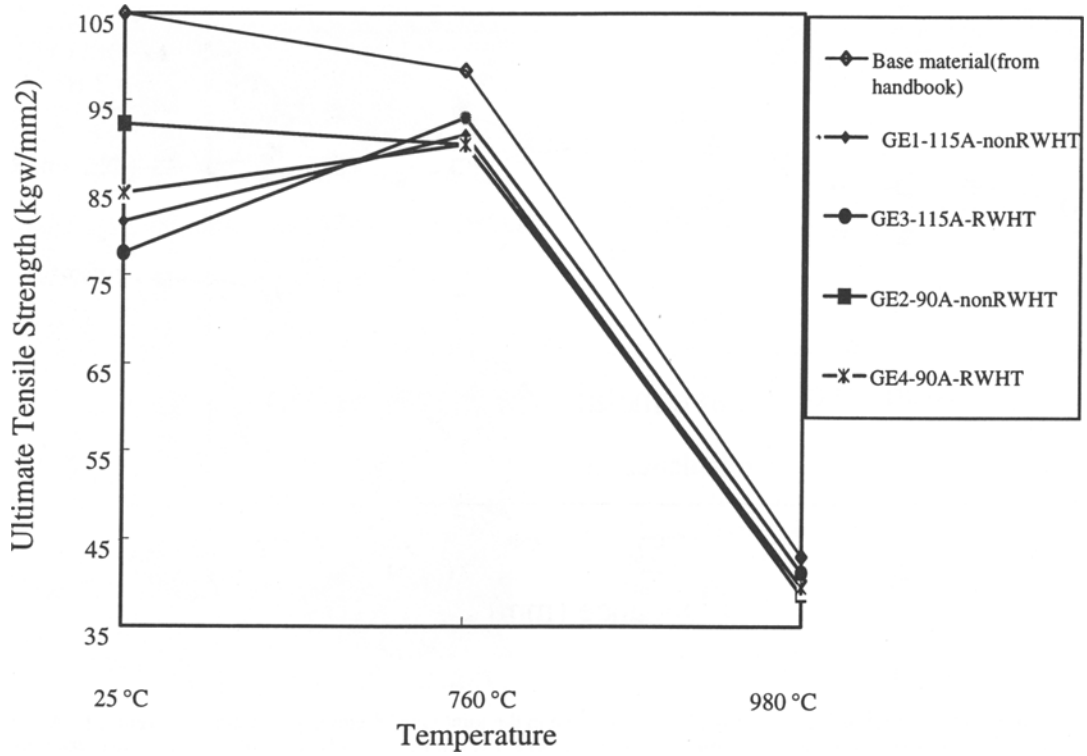

Fig. 13 Ultimate tensile strength (UTS) of PTA-welded IN-738LC at 25, 760 and 980 °C. (UTS of base material was referred from Ref 11)

- The results of tensile tests showed that PTA welded specimens exhibited 96% nominal ultimate tensile strength of IN-738LC base materials. Specimen failure was observed predominantly in the base materials.

References

1. C.T. Sims, N.S. Stoloff, and W.C. Hagel, *Superalloys II,* John Wiley & Sons, 1987
2. D. McKeown, *Weld. J.,* Vol 3, 1971, p 201s
3. K.C. Wu and R.E. Herfert, *Weld. J.,* Vol 1, 1967, p 32s
4. W.P. Hughes and T.F. Berry, *Weld J.,* Vol 8, 1967, p 361s
5. E.G. Thompson, Weld.J., Vol 48 (No. 2), 1969, p 705s
6. M.J. Flether, *Weld. Met. Fabr.,* Vol 38 (No. 2), 1970, p 113
7. W.A. Owczarski, D.S. Duvall, and C.P. Sullivan, *Weld. J.,* No. 4, 1966, p 145s
8. M. Prager and C.S. Shira, *Weld. Res. Counc. Bull.,* No. 128, 1968
9. B. Jahnke, *Weld. J.,* No. 11, 1982, p 343s
10. *PTA Training Manual,* Deloro Stellite, 1992
11. *Aerospace Structure Metals Handbook (V),* Code 4217, Metals and Ceramics Information Center Battelle Columbus Laboratories, 1991
12. P. Burgardt and C.R. Heiple, *Weld. J.,* No. 6, 1986, p 150s
13. S. Kuo, *Welding Metallurgy,* John Wiley & Sons, 1987, p 102